

# Influence of chemical potential on the Casimir-Polder interaction between an atom and gapped graphene or graphene-coated substrate

C. Henkel,<sup>1</sup> G. L. Klimchitskaya,<sup>2,3</sup> and V. M. Mostepanenko<sup>2,3,4</sup>

<sup>1</sup>*Institute of Physics and Astronomy, University of Potsdam,  
Karl-Liebknecht-Straße 24/25, 14476, Potsdam, Germany*

<sup>2</sup>*Central Astronomical Observatory at Pulkovo of the Russian  
Academy of Sciences, Saint Petersburg, 196140, Russia*

<sup>3</sup>*Institute of Physics, Nanotechnology and Telecommunications,  
Peter the Great Saint Petersburg Polytechnic University, Saint Petersburg, 195251, Russia*

<sup>4</sup>*Kazan Federal University, Kazan, 420008, Russia*

## Abstract

We present a formalism based on first principles of quantum electrodynamics at nonzero temperature which permits to calculate the Casimir-Polder interaction between an atom and a graphene sheet with arbitrary mass gap and chemical potential, including graphene-coated substrates. The free energy and force of the Casimir-Polder interaction are expressed via the polarization tensor of graphene in (2+1)-dimensional space-time in the framework of the Dirac model. The obtained expressions are used to investigate the influence of the chemical potential of graphene on the Casimir-Polder interaction. Computations are performed for an atom of metastable helium interacting with either a free-standing graphene sheet or a graphene-coated substrate made of amorphous silica. It is shown that the impacts of the nonzero chemical potential and the mass gap on the Casimir-Polder interaction are in opposite directions by increasing and decreasing the magnitudes of the free energy and force, respectively. It turns out, however, that the temperature-dependent part of the Casimir-Polder interaction is decreased by a nonzero chemical potential, whereas the mass gap increases it compared to the case of undoped, gapless graphene. The physical explanation for these effects is provided. Numerical computations of the Casimir-Polder interaction are performed at various temperatures and atom-graphene separations.

## I. INTRODUCTION

With the advent of graphene, which is a two-dimensional sheet of carbon atoms packed in a hexagonal lattice, it has found widespread application in both fundamental and applied physics [1, 2]. One of the subjects of much recent attention is the interaction of graphene with the zero-point and thermal fluctuations of the electromagnetic field giving rise to the van der Waals (Casimir) and Casimir-Polder forces [3, 4]. These forces act between two graphene sheets and an atom and a graphene sheet (or graphene-coated substrate), respectively. Given that the optical properties of graphene can be modified by doping, it may be possible to tune both the van der Waals (Casimir) and Casimir-Polder interactions. The van der Waals and Casimir interactions between two graphene sheets, a graphene sheet and a 3D-material plate, and graphene-coated substrates have been investigated in the framework of the Dirac model. This model assumes that at low energies the graphene quasiparticles obey a linear dispersion relation but move with the Fermi velocity  $v_F \approx c/300$  rather than with the speed of light [1, 2, 5]. A lot of calculations were performed using the density-density correlation functions, the Kubo formalism, and some special models for the dielectric permittivity (conductivity) of graphene [6–19]. The same methods have been used to calculate the Casimir-Polder force between different atoms and graphene sheet under various conditions [20–25]. Specifically, in Ref. [25] the Casimir-Polder interaction between an atom and a substrate coated with a charge layer was considered. This layer characterized by a nonlocal dielectric response can be used as a simplified model of a graphene sheet.

In the framework of the Lifshitz theory of dispersion forces [2, 26], the Casimir and Casimir-Polder interactions can be expressed in terms of the reflection coefficients for electromagnetic fluctuations. Within the Dirac model, the reflection coefficients of graphene are expressed via a polarization tensor in (2+1)-dimensional space-time [27, 28]. This model allows for both zero and nonzero quasiparticle mass  $m$ . The latter may arise due to electron-electron interactions, impurities and the presence of a substrate. The polarization tensor of Refs. [27, 28] has been used to calculate the Casimir force in many physical systems incorporating graphene sheets for any mass gap  $\Delta = 2mc^2$  and at any temperature [27–32], but it is restricted to the case of undoped graphene (chemical potential  $\mu = 0$ ). The computational results were found [33, 34] to be in a very good agreement with the experimental data of the work on measuring the gradient of the Casimir force between an Au-coated

sphere and a graphene-coated substrate [35]. The same polarization tensor was applied to investigate the Casimir-Polder interaction of different atoms with gapped graphene [36–39] and with graphene-coated plates made of different materials [40]. The classical limit of the Casimir-Polder interaction with graphene systems has also been considered [41].

The polarization tensor of graphene of Ref. [28] is restricted to the purely imaginary Matsubara frequencies. Another representation that provides the analytic continuation to the entire complex frequency plane was derived in Ref. [42]. This representation has been used to investigate the thermal Casimir force in graphene systems [43–46], the electrical conductivity of both gapless and gapped graphene [47, 48], and the reflectivity properties of graphene and graphene-coated substrates [42, 49–51].

Real graphene samples are always doped and can be characterized by a nonzero chemical potential  $\mu$  [5]. Because of this, it is desirable to describe the Casimir and Casimir-Polder forces in graphene systems with account of both parameters  $\Delta$  and  $\mu$ . In Ref. [52] the polarization tensor of graphene found in Ref. [42] was generalized for the case of doped graphene with nonzero chemical potential. According to Ref. [52], the thermal Casimir force between the doped but gapless graphene sheet and an ideal-metal plane can be enhanced up to 60% in comparison to the case of undoped graphene. The detailed investigation of the thermal Casimir force in graphene systems with nonzero mass gap and chemical potential demonstrated that these parameters act in the opposite directions by decreasing and increasing the force magnitude, respectively [53]. However, the role of the chemical potential in the Casimir-Polder interaction between an atom and a graphene sheet or a graphene-coated substrate remained unexplored.

In this paper, we investigate the Casimir-Polder interaction between an atom and a graphene sheet or a graphene-coated substrate in thermal equilibrium with the environment. Graphene is described in the framework of the Dirac model by the polarization tensor taking into account the mass gap and chemical potential at any temperature. In doing so, we consider not too small atom-graphene separations in order to remain in the application region of the Dirac model, where the dispersion relation for graphene quasiparticles remains linear (this holds at energies below 1–2 eV [5, 28, 54]). The material of a substrate is described by a local isotropic dielectric function.

We present the expressions for the Casimir-Polder free energy and force based on first principles of quantum electrodynamics at nonzero temperature. The expressions are used

to compute the Casimir-Polder interaction between an atom of metastable helium  $\text{He}^*$  and a graphene sheet characterized by various values of the mass gap and chemical potential. This atom has a relatively large polarizability and has been used in quantum reflection experiments that are sensitive to the atom-surface interaction [55, 56]. Similar computations are performed for an atom of  $\text{He}^*$  interacting with a graphene-coated  $\text{SiO}_2$  substrate. All computations are made at room temperature and at liquid nitrogen temperature. It is shown that with increasing mass gap or chemical potential the magnitudes of both the Casimir-Polder free energy and force decrease or increase, respectively. Thus, the impacts of both parameters on the Casimir-Polder interaction are in the opposite directions and partially compensate each other. This result is important from the experimental point of view. From the theoretical viewpoint, the temperature dependence of the Casimir-Polder force has attracted much interest, but usually manifests itself at relatively large distance. For graphene, the situation is more favorable because the thermal regime is reached at shorter distances (well below one micrometer). We find that a larger chemical potential suppresses the role of thermal correction at all separations. By contrast, for a larger mass gap the thermal effect is larger. For a graphene-coated substrate, the Casimir-Polder interaction is stronger than for a bare substrate, in particular if the latter is dielectric, but possesses similar physical properties compared to a free-standing graphene sheet.

The paper is organized as follows. In Sec. II, the exact formalism is presented including the analytic expressions for the Casimir-Polder free energy and force in terms of the polarization tensor of graphene with nonzero  $\Delta$  and  $\mu$ . Section III contains the results of numerical computations of the Casimir-Polder free energy and force between an atom of  $\text{He}^*$  and a free-standing graphene sheet. In Sec. IV, similar results for an atom of  $\text{He}^*$  interacting with a graphene-coated  $\text{SiO}_2$  substrate are presented. Section V contains our conclusions and a discussion.

## II. EXACT FORMALISM IN THE FRAMEWORK OF DIRAC MODEL

We consider an atom characterized by the frequency-dependent isotropic electric dipole polarizability  $\alpha(\omega)$  at a distance  $a$  from a graphene sheet deposited on a thick material substrate (semispace) described by the frequency-dependent dielectric permittivity  $\varepsilon(\omega)$ . Graphene is characterized by the mass-gap parameter  $\Delta = 2mc^2$ , where  $m$  is the mass of

quasiparticles, and chemical potential  $\mu$ . The considered system is assumed to be in thermal equilibrium with the environment at temperature  $T$ . The Casimir-Polder free energy of an atom interacting with a graphene-coated substrate is given by the Lifshitz formula [4, 26] which we present in terms of the dimensionless variables

$$\begin{aligned}\mathcal{F}(a, T) &= -k_B T \sum'_{l=0}^{\infty} \alpha(i\zeta_l \omega_c) \text{tr} G(a, i\zeta_l \omega_c), \\ \text{tr} G(a, i\zeta_l \omega_c) &= \frac{1}{8a^3} \int_{\zeta_l}^{\infty} dy e^{-y} \{2y^2 R_{\text{TM}}(i\zeta_l, y) - \zeta_l^2 [R_{\text{TM}}(i\zeta_l, y) + R_{\text{TE}}(i\zeta_l, y)]\}.\end{aligned}\quad (1)$$

Here,  $k_B$  is the Boltzmann constant, the prime on the summation sign indicates that the term with  $l = 0$  is divided by two, and the dimensionless Matsubara frequencies are  $\zeta_l = \xi_l/\omega_c$ , where  $\xi_l = 2\pi k_B T l/\hbar$  with  $l = 0, 1, 2, \dots$  are the dimensional Matsubara frequencies and  $\omega_c = c/(2a)$ . The electromagnetic Green tensor  $G$  (the free-space contribution to  $G$  is subtracted) describes how the field emitted by the atomic dipole is reflected by the surface, as encoded in the reflection amplitudes  $R_{\text{TM}}$  and  $R_{\text{TE}}$  for two independent polarizations, transverse magnetic (TM) and transverse electric (TE). Note that the dimensionless integration variable  $y$  is connected with the magnitude of the projection of the wave vector on the plane of graphene,  $k_{\perp}$ , by  $y = 2aq_l$  where  $q_l^2 = k_{\perp}^2 + \xi_l^2/c^2$ .

The remaining undefined quantities in Eq. (1) are the reflection coefficients. They are expressed through the dielectric permittivity of a substrate material  $\varepsilon_l \equiv \varepsilon(i\xi_l) = \varepsilon(i\zeta_l \omega_c)$  and the dimensionless polarization tensor of graphene  $\tilde{\Pi}_{\beta\gamma}$  with  $\beta, \gamma = 0, 1, 2$  connected with the dimensional tensor  $\Pi_{\beta\gamma}$  by

$$\tilde{\Pi}_{\beta\gamma, l} \equiv \tilde{\Pi}_{\beta\gamma}(i\zeta_l, y) = \frac{2a}{\hbar} \Pi_{\beta\gamma}(i\xi_l, k_{\perp}). \quad (2)$$

As the two independent components of  $\Pi_{\beta\gamma}$ , it is customary to choose  $\Pi_{00}$  and  $\text{tr}\Pi$ , where  $\text{tr}\Pi = \Pi_{\beta}^{\beta}$  is the trace of the polarization tensor. For our purposes, however, it is more convenient to consider, instead of  $\text{tr}\Pi$ , the following combination

$$\Pi_l = k_{\perp}^2 \text{tr}\Pi_l - q_l^2 \Pi_{00, l}. \quad (3)$$

In terms of the dimensionless quantities, Eq. (3) reduces to

$$\tilde{\Pi}_l = \frac{(2a)^3}{\hbar} \tilde{\Pi}_l = (y^2 - \zeta_l^2) \text{tr}\tilde{\Pi}_l - y^2 \tilde{\Pi}_{00, l}. \quad (4)$$

The polarization tensor is directly connected with the nonlocal dielectric permittivities along the graphene surface (the longitudinal one) and perpendicular to it (the transverse

one) [32]

$$\begin{aligned}\varepsilon_{\text{long}}(i\xi_l, k_\perp) &= 1 + \frac{1}{2\hbar k_\perp} \Pi_{00}(i\xi_l, k_\perp), \\ \varepsilon_{\text{tr}}(i\xi_l, k_\perp) &= 1 + \frac{c^2}{2\hbar k_\perp \xi_l^2} \Pi(i\xi_l, k_\perp).\end{aligned}\quad (5)$$

Taking into account the importance of the reflection coefficients in this formalism, we present them first in terms of dimensional variables [33, 53]

$$\begin{aligned}R_{\text{TM}}(i\xi_l, k_\perp) &= \frac{\varepsilon_l q_l - k_l + \frac{q_l k_l \Pi_{00,l}}{\hbar k_\perp^2}}{\varepsilon_l q_l + k_l + \frac{q_l k_l \Pi_{00,l}}{\hbar k_\perp^2}}, \\ R_{\text{TE}}(i\xi_l, k_\perp) &= \frac{q_l - k_l - \frac{\Pi_l}{\hbar k_\perp^2}}{q_l + k_l + \frac{\Pi_l}{\hbar k_\perp^2}},\end{aligned}\quad (6)$$

where  $k_l = \sqrt{k_\perp^2 + \varepsilon_l \xi_l^2 / c^2}$ .

For the case of an atom interacting with a free-standing graphene sheet, we put  $\varepsilon_l = 1$  and Eq. (6) simplifies to [28, 57]

$$\begin{aligned}R_{\text{TM}}(i\xi_l, k_\perp) &= \frac{q_l \Pi_{00,l}}{q_l \Pi_{00,l} + 2\hbar k_\perp^2}, \\ R_{\text{TE}}(i\xi_l, k_\perp) &= -\frac{\Pi_l}{\Pi_l + 2\hbar k_\perp^2 q_l}.\end{aligned}\quad (7)$$

If there is no graphene coating,  $\Pi_{00,l} = \Pi_l = 0$ , and Eq. (6) returns us back to the standard (Fresnel) reflection coefficients.

In terms of dimensionless variables introduced above, Eq. (6) takes the form

$$\begin{aligned}R_{\text{TM}}(i\zeta_l, y) &= \frac{\varepsilon_l y(y^2 - \zeta_l^2) + \sqrt{y^2 + (\varepsilon_l - 1)\zeta_l^2} \left[ y \tilde{\Pi}_{00,l} - (y^2 - \zeta_l^2) \right]}{\varepsilon_l y(y^2 - \zeta_l^2) + \sqrt{y^2 + (\varepsilon_l - 1)\zeta_l^2} \left[ y \tilde{\Pi}_{00,l} + (y^2 - \zeta_l^2) \right]}, \\ R_{\text{TE}}(i\zeta_l, y) &= \frac{(y^2 - \zeta_l^2)[y - \sqrt{y^2 + (\varepsilon_l - 1)\zeta_l^2}] - \tilde{\Pi}_l}{(y^2 - \zeta_l^2)[y + \sqrt{y^2 + (\varepsilon_l - 1)\zeta_l^2}] + \tilde{\Pi}_l}\end{aligned}\quad (8)$$

and Eq. (7) can be written as

$$\begin{aligned}R_{\text{TM}}(i\zeta_l, y) &= \frac{y \tilde{\Pi}_{00,l}}{y \tilde{\Pi}_{00,l} + 2(y^2 - \zeta_l^2)}, \\ R_{\text{TE}}(i\zeta_l, y) &= -\frac{\tilde{\Pi}_l}{\tilde{\Pi}_l + 2y(y^2 - \zeta_l^2)}.\end{aligned}\quad (9)$$

The explicit expressions for  $\tilde{\Pi}_{00,l}$  and  $\tilde{\Pi}_l$  for graphene with nonzero chemical potential were found in Ref. [52] and used in Ref. [53] to investigate the joint action of  $\Delta$  and  $\mu$  on

the thermal Casimir force. By using the dimensionless variables  $y$  and  $\zeta_l$ , we represent the respective equations of Ref. [53] in a more simple form. At first it is convenient to write the quantities  $\tilde{\Pi}_{00,l}$  and  $\tilde{\Pi}_l$  as sums of two contributions

$$\begin{aligned}\tilde{\Pi}_{00,l}(y, T, m, \mu) &= \tilde{\Pi}_{00,l}^{(0)}(y, m) + \tilde{\Pi}_{00,l}^{(1)}(y, T, m, \mu), \\ \tilde{\Pi}_l(y, T, m, \mu) &= \tilde{\Pi}_l^{(0)}(y, m) + \tilde{\Pi}_l^{(1)}(y, T, m, \mu),\end{aligned}\quad (10)$$

where the first terms on the right-hand side refer to undoped graphene with  $\mu = 0$  at zero temperature, whereas the second ones account for the thermal effect and for the dependence on  $\mu$ . Note that  $\tilde{\Pi}_{00,l}^{(1)}$  and  $\tilde{\Pi}_l^{(1)}$  may remain different from zero even in the limiting case  $T \rightarrow 0$  and, thus, have no meaning of thermal corrections.

The explicit form for  $\tilde{\Pi}_{00,l}^{(0)}$  and  $\tilde{\Pi}_l^{(0)}$  is the following [27, 28, 53]

$$\begin{aligned}\tilde{\Pi}_{00,l}^{(0)}(y, m) &= \alpha \frac{y^2 - \zeta_l^2}{p_l} \Psi(D_l), \\ \tilde{\Pi}_l^{(0)}(y, m) &= \alpha (y^2 - \zeta_l^2) p_l \Psi(D_l),\end{aligned}\quad (11)$$

where  $\alpha = e^2/(\hbar c)$  is the fine structure constant,  $D_l = 4mca/(\hbar p_l)$ ,

$$\begin{aligned}\Psi(x) &= 2 \left[ x + (1 - x^2) \arctan \frac{1}{x} \right], \\ p_l \equiv p_l(y) &= \sqrt{\tilde{v}_F^2 y^2 + (1 - \tilde{v}_F^2) \zeta_l^2},\end{aligned}\quad (12)$$

and the dimensionless Fermi velocity is  $\tilde{v}_F = v_F/c \approx 1/300$ .

The explicit expressions for the second terms on the right-hand side of Eq. (10) were derived in Ref. [52] (see also Ref. [53] for an equivalent representation). Using the dimensionless variables, they can be written as

$$\begin{aligned}\tilde{\Pi}_{00,l}^{(1)}(y, T, m, \mu) &= \frac{4\alpha p_l}{\tilde{v}_F^2} \int_{D_l}^{\infty} du w_l(u, y, T, \mu) \\ &\times \left\{ 1 - \operatorname{Re} \frac{p_l - p_l u^2 + 2i\zeta_l u}{[p_l^2 - p_l^2 u^2 + \tilde{v}_F^2 (y^2 - \zeta_l^2) D_l^2 + 2i\zeta_l p_l u]^{1/2}} \right\}, \\ \tilde{\Pi}_l^{(1)}(y, T, m, \mu) &= -\frac{4\alpha p_l}{\tilde{v}_F^2} \int_{D_l}^{\infty} du w_l(u, y, T, \mu) \\ &\times \left\{ \zeta_l^2 - p_l \operatorname{Re} \frac{\zeta_l^2 - p_l^2 u^2 + \tilde{v}_F^2 (y^2 - \zeta_l^2) D_l^2 + 2i\zeta_l p_l u}{[p_l^2 - p_l^2 u^2 + \tilde{v}_F^2 (y^2 - \zeta_l^2) D_l^2 + 2i\zeta_l p_l u]^{1/2}} \right\}.\end{aligned}\quad (13)$$

Here, we have used the notation

$$\begin{aligned}w_l(u, y, T, \mu) &= \frac{1}{e^{B_l u + \frac{\mu}{k_B T}} + 1} + \frac{1}{e^{B_l u - \frac{\mu}{k_B T}} + 1}, \\ B_l \equiv B_l(y, T) &= \frac{\hbar c}{4ak_B T} p_l(y),\end{aligned}\quad (14)$$

where  $p_l$  is defined in Eq. (12).

As is seen in Eq. (13), the expressions for  $\tilde{\Pi}_{00,l}^{(1)}$  and  $\tilde{\Pi}_l^{(1)}$  with  $l \geq 1$  are much more complicated than with  $l = 0$ , and it is convenient to deal with them separately. Using Eqs. (10), (11), and (13), we first present the total quantities  $\tilde{\Pi}_{00,l}$  and  $\tilde{\Pi}_l$  at  $l = 0$

$$\begin{aligned}
\tilde{\Pi}_{00,0}(y, T, m, \mu) &= \frac{\alpha y}{\tilde{v}_F} \Psi(D_0) + \frac{16\alpha a k_B T}{\tilde{v}_F^2 \hbar c} \\
&\times \ln \left[ \left( e^{\frac{\mu}{k_B T}} + e^{-\frac{mc^2}{k_B T}} \right) \left( e^{-\frac{\mu}{k_B T}} + e^{-\frac{mc^2}{k_B T}} \right) \right] \\
&- \frac{4\alpha y}{\tilde{v}_F} \int_{D_0}^{\sqrt{1+D_0^2}} du w_0(u, y, T, \mu) \frac{1-u^2}{(1-u^2+D_0^2)^{1/2}}, \\
\tilde{\Pi}_0(y, T, m, \mu) &= \alpha \tilde{v}_F y^3 \Psi(D_0) \\
&+ 4\alpha \tilde{v}_F y^3 \int_{D_0}^{\sqrt{1+D_0^2}} du w_0(u, y, T, \mu) \frac{-u^2+D_0^2}{(1-u^2+D_0^2)^{1/2}},
\end{aligned} \tag{15}$$

where

$$D_0 = \frac{2a\Delta}{\hbar v_F y}, \quad B_0 = \frac{\hbar v_F y}{4a k_B T}. \tag{16}$$

For  $l \geq 1$  one can use much simpler approximate expressions for  $\tilde{\Pi}_{00,l}^{(1)}$  and  $\tilde{\Pi}_l^{(1)}$  than those presented in Eq. (13) with no loss in accuracy. It was shown that for all  $l \geq 1$  under the condition  $\zeta_1 \gg \tilde{v}_F$  [which is equivalent to  $k_B T \gg \hbar v_F / (4\pi a)$ ] Eqs. (10), (11) and (13) lead to [43, 53]

$$\begin{aligned}
\tilde{\Pi}_{00,l}(y, T, m, \mu) &\approx \frac{\alpha(y^2 - \zeta_l^2)}{\zeta_l} \\
&\times \left[ \Psi \left( \frac{4mca}{\hbar \zeta_l} \right) + \tilde{Y}_l(y, T, m, \mu) \right], \\
\tilde{\Pi}_l(y, T, m, \mu) &\approx \alpha \zeta_l (y^2 - \zeta_l^2) \\
&\times \left[ \Psi \left( \frac{4mca}{\hbar \zeta_l} \right) + \tilde{Y}_l(y, T, m, \mu) \right],
\end{aligned} \tag{17}$$

where

$$\tilde{Y}_l(y, T, m, \mu) = 2 \int_{\frac{4mca}{\hbar \zeta_l}}^{\infty} du w_l(u, y, T, \mu) \frac{u^2 + \left( \frac{4mca}{\hbar \zeta_l} \right)^2}{u^2 + 1}. \tag{18}$$

Note that for  $a = 50$  nm at  $T = 300$  K the first dimensionless Matsubara frequency  $\zeta_1$  is larger than  $\tilde{v}_F$  by a factor of 25 (and more for larger separations). Because of this, the use of the approximate expression (17) leads to practically exact Casimir-Polder free energy and force (the relative error is less than 0.02% [43]) if the zero-frequency contributions to them are calculated using the exact Eq. (15). Computations show that even at liquid nitrogen



temperature ( $T = 77.2$  K) for  $a > 50$  nm ( $\zeta_1/\tilde{v}_F > 6.4$ ) the use of Eq. (17) for  $l \geq 1$  allows computation of the Casimir-Polder interaction accurate to a fraction of a percent.

As an illustration, in Fig. 1 we present (a) the 00-component of the polarization tensor,  $\Pi_{00}(i\xi, k_\perp)$ , and (b) the quantity  $\Pi(i\xi, k_\perp)$  defined in Eq. (3) as functions of  $\xi/\xi_1$ , where  $\xi$  varies along the imaginary frequency axis and  $\xi \geq \xi_1$ . Computations are performed using Eqs. (2), (4), (15), and (17) for a gapless graphene ( $m = 0$ ) at  $k_\perp = 10\xi_1/c$  at room temperature  $T = 300$  K (the solid lines) and at liquid nitrogen temperature  $T = 77$  K (the dashed lines). The lines of each kind from bottom to top are plotted for the chemical potential  $\mu = 0, 0.2, \text{ and } 0.5$  eV, respectively (see the discussion of typical values taken by the chemical potential of graphene samples in Sec. III). At zero Matsubara frequency  $\Pi_{00}$  takes the values  $0.507, 11.0, \text{ and } 27.5 \mu\text{eV s/m}$  ( $T = 77$  K) and  $1.97, 11.0, \text{ and } 27.5 \mu\text{eV s/m}$  ( $T = 300$  K) for  $\mu = 0, 0.2, \text{ and } 0.5$  eV, respectively. The quantity  $\Pi$  at zero Matsubara frequency takes the values  $0.021, 0, \text{ and } 0 \text{ eV s/m}^3$  ( $T = 77$  K) and  $1.25, 0.0022, \text{ and } 0 \text{ eV s/m}^3$  ( $T = 300$  K) for  $\mu = 0, 0.2, \text{ and } 0.5$  eV, respectively. As is seen in Fig. 1, the quantity  $\Pi_{00}$  decreases and the quantity  $\Pi$  increases monotonously with increase of  $\xi$ . In all cases the magnitudes of both  $\Pi_{00}$  and  $\Pi$  are larger for higher temperature and larger chemical potential. From Figs. 1(a) and 1(b) one can conclude that the impact of  $\mu$  on the values of  $\Pi_{00}$  and  $\Pi$  decreases with increasing frequency.

As a result, the Casimir-Polder free energy of an atom interacting with a free-standing graphene sheet or graphene-coated substrate can be computed by Eqs. (1) and (8) or (9) where the polarization tensor is given in Eqs. (10), (11) and (13) or (15) and (17). To calculate the respective Casimir-Polder force, one should use the following Lifshitz formula [4]:

$$F(a, T) = -\frac{k_B T}{8a^4} \sum_{l=0}^{\infty} \alpha(i\zeta_l \omega_c) \int_{\zeta_l}^{\infty} y dy e^{-y} \quad (19)$$

$$\times \{2y^2 R_{\text{TM}}(i\zeta_l, y) - \zeta_l^2 [R_{\text{TM}}(i\zeta_l, y) + R_{\text{TE}}(i\zeta_l, y)]\}$$

in place of Eq. (1).

### III. INTERACTION WITH FREE-STANDING DOPED GRAPHENE SHEET

Here, we calculate the Casimir-Polder free energy and force for an atom of metastable helium ( $\text{He}^*$ ) interacting with a free-standing graphene sheet. All computations are per-

formed by using Eqs. (1) and (19) where the reflection coefficients are given by Eq. (9) and the polarization tensor by Eqs. (15) and (17), and we vary the mass-gap parameter and the chemical potential. These computations require data for the He\* polarizability  $\alpha(i\xi)$  as a function of imaginary frequency. Below we use the highly accurate polarizability of Refs.[58, 59] which has a relative error of order of  $10^{-6}$ . It is shown in Fig. 2 by the solid line as a function of frequency, normalized to its static value  $\alpha(0) = 46.7727 \text{ \AA}^3$  [60]. Note that the dynamic polarizability is often represented using the single-oscillator model [59–62]

$$\alpha(i\xi) = \frac{\alpha(0)}{1 + \frac{\xi^2}{\omega_0^2}}, \quad (20)$$

where for He\* one has  $\omega_0 = 1.793 \times 10^{15} \text{ rad/s}$  [60]. In Fig. 2, the latter one is shown by the dashed line, and it is seen that the major deviations between the highly accurate and the single-oscillator data for the dynamic polarizability occur in the region of high frequencies (see inset at an enlarged scale). This corresponds to the atom–graphene separations of order of 10 nm or shorter.

In Fig. 3(a) we present the computational results for the magnitude of the Casimir-Polder free energy as functions of separation. For the ease of representing the data, we multiply them with the third power of separation between an atom of He\* and a graphene sheet. The computations are done for a gapless graphene ( $\Delta = 0$ ) at room temperature  $T = 300 \text{ K}$  (the solid lines) and at liquid nitrogen temperature  $T = 77 \text{ K}$  (the dashed lines). We use a value for the Fermi velocity of  $v_F \approx c/300$ . For the three solid (and three dashed) lines considered from bottom to top the chemical potential of graphene  $\mu$  is equal to 0, 0.2, and 0.5 eV, respectively.

Note that the chemical potential can be expressed via the doping concentration  $n$  [63]

$$\mu = \hbar v_F \sqrt{\pi n}. \quad (21)$$

In Ref. [35],  $n$  was estimated as  $\approx 1.2 \times 10^{10} \text{ cm}^{-2}$  for nearly undoped graphene under high vacuum conditions. This leads to a chemical potential that does not exceed a value of  $\mu \approx 0.02 \text{ eV}$ . The values of  $\mu = 0.2$  and  $0.5 \text{ eV}$  occur for doping concentrations  $n \approx 3 \times 10^{12}$  and  $2 \times 10^{13} \text{ cm}^{-2}$ .

As is seen in Fig. 3(a), the magnitude of the Casimir-Polder free energy quickly decreases with increasing atom-graphene separation. In so doing at all considered separations and temperatures the magnitude of the free energy is larger for graphene with larger chemical

potential. This result is in agreement with the result of Ref. [52] obtained for the Casimir interaction of a graphene sheet with an ideal-metal plane. From Fig. 3(a) it is also seen that the distance between the pair of bottom solid and dashed lines is much larger than between the pair of top ones. This means that the thermal contribution to the Casimir-Polder interaction decreases with increasing chemical potential. Note also that it becomes significant at much shorter distances compared to the Casimir-Polder interaction with a bulk substrate.

In Fig. 3(b) we especially consider the relative change in the Casimir-Polder free energy which occurs when the chemical potential of a graphene sheet becomes not equal to zero

$$\delta_\mu \mathcal{F}(a, T) = \frac{\mathcal{F}(a, T, \mu) - \mathcal{F}(a, T, 0)}{\mathcal{F}(a, T, 0)}. \quad (22)$$

The quantity  $\delta_\mu \mathcal{F}(a, T)$ , as a function of separation, is plotted in Fig. 3(b) at  $T = 300$  K (the solid lines) and  $T = 77$  K (the dashed lines). The solid (and dashed) lines considered from bottom to top correspond to  $\mu = 0.1, 0.2,$  and  $0.5$  eV, respectively. From Fig. 3(b) it can be seen that at lower temperature ( $T = 77$  K) the relative differences in the Casimir-Polder free energy are much larger than at  $T = 300$  K. It is also seen that at  $T = 77$  K all the dashed lines reach the maximum value at some separation, whereas at  $T = 300$  K only the top solid line reaches the maximum value in the considered separation region from 50 nm to 1  $\mu$ m.

Similar results for the Casimir-Polder force computed using Eq. (19) are presented in Fig. 4 using the same parameters and the same notation for all lines. As is seen in Fig. 4(a), the magnitude of the Casimir-Polder force decreases even more quickly than the free energy with increasing separation. At each separation it is larger for larger chemical potential. As it holds for the free energy, the thermal effect in the Casimir-Polder force is larger for graphene with lower chemical potential.

In Fig. 4(b) the relative change in the Casimir-Polder force due to nonzero chemical potential, defined in the same way as in Eq. (22), is plotted as a function of separation at  $T = 300$  K (the solid lines) and  $T = 77$  K (the dashed lines) for  $\mu = 0.1, 0.2,$  and  $0.5$  eV, respectively, when lines are considered from bottom to top. It is seen that, again, the relative impact of nonzero  $\mu$  on the Casimir-Polder force is greater at lower temperature. The maximum values of  $\delta_\mu F$  are reached at larger separations than for  $\delta_\mu \mathcal{F}$ .

Now we consider the Casimir free energy between an atom of He\* and a graphene sheet with different values of mass gap  $\Delta = 2mc^2$  as a function of the chemical potential  $\mu$ . In

fact for a perfect (pristine) graphene the Dirac-type electronic quasiparticles are massless, so that  $m = 0$ ,  $\Delta = 0$ . For real graphene samples, however, the account of interelectron interactions, structural defects, and the presence of a substrate may lead to some nonzero mass gap estimated as  $\Delta \lesssim 0.2$  eV [5, 64–66].

In Fig. 5 we plot the magnitude of the Casimir-Polder free energy between an atom of He\* and a gapped graphene sheet at  $T = 300$  K and  $T = 77$  K as function of the chemical potential  $\mu$  at (a)  $a = 100$  nm and (b)  $a = 500$  nm. For both temperatures, the mass gap is  $\Delta = 0.2, 0.1,$  and  $0$  eV from bottom to top. As is seen in Figs. 5(a) and 5(b), at all values of  $\mu$  and  $T$  an increase of the mass gap results in a decrease in the magnitude of the Casimir-Polder free energy. As to the thermal effect, it becomes larger for graphene sheets with larger mass gap. From Figs. 5(a) and 5(b) it can be seen that the dependence of  $a^3|\mathcal{F}|$  on  $\mu$  exhibits some kind of steps which are better seen in the case of lower temperature (the dashed lines). This is because with decreasing  $T$  the contribution of the first fraction in the first line on the right-hand side of Eq. (14) becomes negligibly small, whereas the major part in the contribution of the second fraction appears under the condition

$$B_l u - \frac{\mu}{k_B T} < 0. \quad (23)$$

Taking into account the definition of  $B_l$  in Eq. (14) and the fact that the integration in Eq. (13) is over the interval  $u \geq D_l$ , we find from Eq. (23) that with decreasing temperature the major contribution to  $\tilde{\Pi}_{00,l}^{(1)}$  and  $\tilde{\Pi}_l^{(1)}$  appears under the condition  $2mc^2 = \Delta < 2\mu$ . If this condition is not satisfied, with decreasing temperature the free energy becomes almost independent on  $\mu$  [53]. The latter explains the characteristic flat regions of the dashed lines in the vicinity of zero  $\mu$ . As to the second steps at nonzero  $\mu$ , which are clearly seen on the dashed lines in Fig. 5(b), they are explained by an interplay between the condition  $\Delta < 2\mu$ , which influences only partially at nonzero temperature, and the role of thermal effects determined by the effective temperature  $T_{\text{eff}} = \hbar v_F / (2ak_B)$ . This takes a value  $T_{\text{eff}} \approx 38$  K at  $a \approx 100$  nm.

Figure 6 demonstrates similar computational results for the magnitude of the Casimir-Polder force multiplied by the fourth power of separation between an atom of He\* and a gapped graphene sheet. All the notations are the same as in Fig. 5. From Figs. 6(a) and 6(b), plotted at  $a = 100$  and  $500$  nm, respectively, it is seen that with increasing mass gap the magnitude of the Casimir-Polder force at some fixed temperature and chemical potential

becomes smaller. The thermal effect in the Casimir-Polder force becomes larger for larger mass-gap parameter. The step structure clearly seen on the dashed lines plotted at  $T = 77$  K is explained by the same reasons as for the Casimir-Polder free energy. It is interesting that at  $a = 100$  nm,  $\mu > 0.04$  eV the Casimir-Polder force calculated at  $T = 77$  K for graphene with  $\Delta = 0$  becomes larger in magnitude than that one at  $T = 300$  K for graphene with  $\Delta = 0.2$  eV [see the top dashed and the bottom solid lines in Fig. 6(a)]. This means that the effect of chemical potential on the Casimir-Polder force can exceed the thermal effect. In a similar way, at  $a = 100$  nm,  $\mu > 0.16$  eV the Casimir-Polder force calculated at  $T = 77$  K for graphene with  $\Delta = 0.1$  eV reaches and remains equal to that one at  $T = 300$  K for graphene with  $\Delta = 0.2$  eV [compare the bottom solid and the first above the bottom dashed lines in Fig. 6(a)].

To conclude this section we note that the thermal dependence of the Casimir-Polder free energy and force consists of two contributions. The first one originates from the summation over the Matsubara frequencies in the Lifshitz formulas (1) and (19) when the polarization tensor at zero temperature is used in computations. The second one is from an explicit temperature dependence of the full polarization tensor defined at nonzero temperature. In Ref. [36] it was shown that for a gapped graphene with zero chemical potential the explicit temperature dependence of the polarization tensor contributes to the thermal Casimir-Polder interaction significantly. Thus, this contribution is equal to 23% of the total Casimir-Polder free energy for a gapless graphene at  $a = 1$   $\mu$ m,  $T = 300$  K, and it increases quickly with increasing mass gap reaching more than 80% of the free energy [36]. Similar situation holds for graphene with nonzero chemical potential satisfying the condition  $2\mu < \Delta$ . Under this condition the chemical potential does not influence the value of the polarization tensor at zero temperature [53], so that

$$\begin{aligned}\tilde{\Pi}_{00,l}(y, 0, m, \mu) &= \tilde{\Pi}_{00,l}^{(0)}(y, m), \\ \tilde{\Pi}_l(y, 0, m, \mu) &= \tilde{\Pi}_l^{(0)}(y, m)\end{aligned}\tag{24}$$

for  $\mu < mc^2$ . In this regime, the quantities  $\tilde{\Pi}_{00,l}^{(1)}$ ,  $\tilde{\Pi}_l^{(1)}$  in Eq. (10) vanish when  $T \rightarrow 0$  and, thus, coincide with the thermal corrections. If, however, the condition  $2\mu > \Delta$  is satisfied, the polarization tensor becomes  $\mu$ -dependent even at zero temperature:

$$\begin{aligned}\tilde{\Pi}_{00,l}(y, 0, m, \mu) &= \tilde{\Pi}_{00,l}^{(0)}(y, m) + \tilde{\Pi}_{00,l}^{(1)}(y, 0, m, \mu), \\ \tilde{\Pi}_l(y, 0, m, \mu) &= \tilde{\Pi}_l^{(0)}(y, m) + \tilde{\Pi}_l^{(1)}(y, 0, m, \mu).\end{aligned}\tag{25}$$

The second terms on the right-hand side of Eq. (25) increase the polarization tensor at  $T = 0$  significantly. As a result, the explicit temperature dependence of the polarization tensor plays a weaker role and the Casimir-Polder free energy and force become temperature-dependent mainly because of the Matsubara summation. Thus, for  $\Delta = 0$  and  $\mu = 0.1$  eV the explicit dependence of the polarization tensor on  $T$  contributes only 0.24% and 0.12% to the total Casimir-Polder free energy at  $a = 100$  nm and  $1$   $\mu$ m, respectively. If  $\mu = 0.2$  eV, this contribution is equal to 0.24% and 0.06% at the same respective separations. One can conclude that with respect to the relative roles of two thermal contributions to the Casimir-Polder free energy, the mass gap and chemical potential again influence in the opposite directions.

In the next section we consider how the above results for the Casimir-Polder free energy and force are modified if the graphene sheet is deposited on a material substrate.

#### IV. INTERACTION WITH SUBSTRATE COATED WITH DOPED GRAPHENE

Here, we consider the Casimir-Polder interaction of a  $\text{He}^*$  atom with a graphene sheet deposited on an amorphous silica ( $\text{SiO}_2$ ) substrate. This material is often used for the deposition of graphene [35, 67]. Computations of the Casimir-Polder free energy and force using Eqs. (1) and (19) with the reflection coefficients (8) require the values of the dielectric permittivity of  $\text{SiO}_2$ ,  $\varepsilon_l$ , at the imaginary Matsubara frequencies. A sufficiently exact approximation for  $\varepsilon_{\text{SiO}_2}$  along the imaginary frequency axis is given by the two-oscillator model [68, 69]

$$\varepsilon_{\text{SiO}_2}(i\xi) = 1 + \frac{C_{\text{UV}}\omega_{\text{UV}}^2}{\xi^2 + \omega_{\text{UV}}^2} + \frac{C_{\text{IR}}\omega_{\text{IR}}^2}{\xi^2 + \omega_{\text{IR}}^2}, \quad (26)$$

with the ‘‘oscillator strengths’’  $C_{\text{UV}} = 1.098$ ,  $C_{\text{IR}} = 1.703$  and ‘‘resonance frequencies’’  $\omega_{\text{UV}} = 2.033 \times 10^{16}$  rad/s, and  $\omega_{\text{IR}} = 1.88 \times 10^{14}$  rad/s.

We begin by considering the change of the Casimir-Polder free energy when the  $\text{SiO}_2$  plate is coated with a graphene sheet. For this purpose we calculate the dimensionless ratio

$$\delta_g \mathcal{F}_{\text{SiO}_2}(a, T) = \frac{\mathcal{F}_{\text{SiO}_2}^g(a, T) - \mathcal{F}_{\text{SiO}_2}(a, T)}{\mathcal{F}_{\text{SiO}_2}(a, T)}, \quad (27)$$

where  $\mathcal{F}_{\text{SiO}_2}^g$  and  $\mathcal{F}_{\text{SiO}_2}$  are the free energies of an atom interacting with the graphene-coated and uncoated  $\text{SiO}_2$  plates, respectively. The quantity  $\mathcal{F}_{\text{SiO}_2}$  is calculated using the same Lifshitz formula (1), as  $\mathcal{F}_{\text{SiO}_2}^g$ , but in the reflection coefficients (8) one should put  $\tilde{\Pi}_{00,l} =$

$\tilde{\Pi}_l = 0$  and obtain

$$R_{\text{TM}}^{\text{SiO}_2}(i\zeta_l, y) = \frac{\varepsilon_l y - \sqrt{y^2 + (\varepsilon_l - 1)\zeta_l^2}}{\varepsilon_l y + \sqrt{y^2 + (\varepsilon_l - 1)\zeta_l^2}},$$

$$R_{\text{TE}}^{\text{SiO}_2}(i\zeta_l, y) = \frac{y - \sqrt{y^2 + (\varepsilon_l - 1)\zeta_l^2}}{y + \sqrt{y^2 + (\varepsilon_l - 1)\zeta_l^2}}. \quad (28)$$

First, we focus on gapless ( $\Delta = 0$ ) graphene and vary the chemical potential.

In Fig. 7(a), the computational results for the relative change  $\delta_g \mathcal{F}_{\text{SiO}_2}$  due to the presence of graphene are shown as functions of separation by the solid and dashed lines at  $T = 300$  K and  $77$  K, respectively. Both the solid and dashed lines, considered from the bottom one to the top one, correspond to the chemical potential, equal to  $0, 0.1, 0.2,$  and  $0.5$  eV, respectively. As is seen in Fig. 7(a), the Casimir–Polder free energy increases in magnitude by coating the silica substrate with graphene. For each value of  $\mu$  the quantity  $\delta_g \mathcal{F}_{\text{SiO}_2}$  reaches a minimum value at rather short separations and then increases with increasing  $a$  rather quickly (at  $T = 300$  K) or slowly (at  $T = 77$  K). For larger  $\mu$  the relative change  $\delta_g \mathcal{F}_{\text{SiO}_2}$  takes larger values at all separations.

In Fig. 7(b) the computational results for the relative change  $\delta_\mu \mathcal{F}$  [Eq. (22)] in the Casimir-Polder free energy, which occurs when  $\mu$  becomes not equal to zero, are plotted for the case of gapless graphene deposited on a  $\text{SiO}_2$  substrate. Note that in the definition of this quantity (22)  $\mathcal{F}$  on the right-hand side should be replaced with  $\mathcal{F}_{\text{SiO}_2}^g$  and  $\delta_\mu \mathcal{F}$  with  $\delta_\mu \mathcal{F}_{\text{SiO}_2}$ . The computational results for  $\delta_\mu \mathcal{F}_{\text{SiO}_2}$  are shown in Fig. 7(b) by the solid lines at  $T = 300$  K and by the dashed lines at  $T = 77$  K as functions of separation. The lines of both kinds counted from bottom to top correspond to  $\mu = 0.1, 0.2,$  and  $0.5$  eV, respectively. Note that with decreasing temperature (the dashed lines) the relative change in the Casimir-Polder free energy due to nonzero  $\mu$  for graphene deposited on a substrate becomes almost independent on separation. This is different from the case of a free-standing graphene sheet [see Fig. 3(b)].

Next we consider the dependence of the Casimir free energy on both the chemical potential and mass-gap parameter of graphene coating. In Fig. 8 the magnitudes of the free energy of an atom of  $\text{He}^*$  interacting with a graphene-coated  $\text{SiO}_2$  substrate multiplied by the third power of separation  $a = 0.5 \mu\text{m}$  are plotted by the solid and dashed lines at  $T = 300$  K and  $T = 77$  K, respectively, as functions of (a) chemical potential  $\mu$  and (b) mass-gap parameter  $\Delta$ . The lines of each type counted from bottom to top correspond to (a)  $\Delta = 0.2, 0.1,$  and

0 eV and (b)  $\mu = 0, 0.1, 0.2,$  and  $0.5$  eV.

As is seen in Fig. 8(a), with increasing  $\Delta$  the magnitude of the Casimir-Polder free energy decreases, and this effect is more pronounced at lower temperature. This is in agreement with the case of a free-standing graphene sheet. The comparison of Fig. 8(a) with Fig. 5(b) plotted for a free-standing graphene at the same distance from an atom  $a = 0.5 \mu\text{m}$  shows that for a graphene-coated substrate we have a strong increase in the magnitude of the free energy. This is explained by the role of  $\text{SiO}_2$  substrate. At the same time, the fine structure of the lines (including the steps typical for the dashed lines discussed in Sec. III) is caused by the presence of graphene coating.

From Fig. 8(b) one concludes that the impact of chemical potential on the Casimir-Polder free energy is just the opposite, as compared to the impact of  $\Delta$ . Specifically, with increasing  $\mu$  the magnitude of the free energy  $|\mathcal{F}_{\text{SiO}_2}^g|$  increases and the thermal correction becomes smaller. With increasing mass-gap parameter,  $|\mathcal{F}_{\text{SiO}_2}^g|$  decreases slowly when the chemical potential is relatively large ( $\mu = 0.5$  or  $0.2$  eV) and more rapidly for  $\mu = 0.1$  eV or for undoped graphene.

Similar computations have been performed for the Casimir-Polder force between an atom of  $\text{He}^*$  and a graphene-coated  $\text{SiO}_2$  substrate. Using the same notations, as in Fig. 8, the computational results for the magnitude of the Casimir-Polder force multiplied by the fourth power of separation  $a = 0.5 \mu\text{m}$  are shown as functions of the chemical potential  $\mu$  in Fig. 9(a) and as functions of the mass-gap parameter in Fig. 9(b). As can be seen in Figs. 9(a) and 9(b), qualitatively the character of the quantity  $a^4|F_{\text{SiO}_2}^g|$  is the same as  $a^3|\mathcal{F}_{\text{SiO}_2}^g|$ . Specifically, the increase of  $\mu$  and  $\Delta$  impact on  $|F_{\text{SiO}_2}^g|$  in the opposite directions by increasing and decreasing it, respectively. The comparison of Fig. 9(a) with Fig. 6(b) again demonstrates that the main contribution to the force magnitude is given by the substrate, whereas the fine structure of the force lines is caused by the graphene coating. We also note that the lines for the Casimir-Polder force for 77 K and 300 K cross [compare the top dashed line with the bottom solid line in Fig. 9(b)]. This illustrates the wide tuning range that becomes available by changing the chemical potential.



## V. CONCLUSION AND DISCUSSION

In this paper we have investigated the Casimir-Polder interaction between an atom and a free-standing graphene sheet characterized by some chemical potential and mass-gap parameter. The interaction of an atom with a graphene-coated substrate was also considered. For this purpose, we used the exact formalism of the polarization tensor in (2+1)-dimensional space-time, developed in the framework of the Dirac model. This approach permits a detailed analysis of the impact of nonzero chemical potential of gapped graphene on the Casimir-Polder free energy and force at arbitrary temperature at not too short separations between an atom and a graphene sheet or a graphene-coated substrate. Keeping in mind that during the last few years the Casimir-Polder interaction has found numerous and diverse applications (see, e.g., Refs. [55, 56, 70–78]), the elaboration of the corresponding theoretical formalism for graphene, started in Refs. [20–25, 36–41], should be considered as rather promising.

The developed theory was applied to compute the Casimir-Polder free energy and force between an atom of metastable helium  $\text{He}^*$  and graphene sheets with various values of the chemical potential  $\mu$  and mass-gap parameter  $\Delta$ . These computations have been made possible by the use of Eq. (9) combined with Eqs. (15) and (17) accounting for the mass gap and chemical potential. It was shown that with increasing  $\mu$  the magnitudes of both the Casimir-Polder free energy and force increase. By contrast, with increasing  $\Delta$  the magnitudes of both the free energy and force decrease. Thus, the impacts of nonzero  $\mu$  and  $\Delta$  on the Casimir-Polder interaction in real graphene samples partially compensate each other. It was also shown that for graphene with larger  $\mu$  the thermal effect in the Casimir-Polder interaction is smaller, whereas for graphene with larger mass gap  $\Delta$  the thermal effect is larger.

The obtained results can be understood qualitatively on simple physical grounds. The point is that by increasing  $\mu$  the size of the Fermi surface grows, thus increasing the density of charge carriers and the electrical conductivity of graphene. It is then quite natural that the reflection amplitudes and the Casimir-Polder force increase in magnitude. By contrast, an increase of the mass gap decreases the mobility of charge carriers, which, in turn, decreases the conductivity and, thus, the force magnitude. We have also found that with decreasing temperature the functional dependences of both the Casimir-Polder free energy and force possess some kind of step structure depending on the relationship between the values of  $\Delta$

and  $2\mu$ .

Similar computations of the Casimir-Polder free energy and force have been performed for an atom of  $\text{He}^*$  interacting with a graphene sheet deposited on a  $\text{SiO}_2$  substrate. These computations have been made possible by the use of Eq. (8) combined with Eqs. (15) and (17). Qualitatively the same results, as for a free-standing graphene sheet, were obtained with the only difference that the magnitudes of both the Casimir-Polder free energy and force are much larger due to the role of a substrate. Specifically, it was shown that the nonzero chemical potential and mass gap act on the Casimir-Polder interaction in the opposite directions and partially compensate each other.

The obtained results allow a reliable calculation of the Casimir-Polder interaction between any atom and real graphene sheets, both free-standing and deposited on substrates made of different materials. These results demonstrate the possibility of tuning the Casimir-Polder interaction over a relatively wide range by changing the doping concentration in graphene. This may be useful for future experiments probing the interaction of atoms with graphene and other two-dimensional nanostructures.

### Acknowledgments

C.H. acknowledges support from the *Deutsche Forschungsgemeinschaft* through the DIP program (grant number Schm-1049/7-1). G.L.K. and V.M.M. thank the University of Potsdam, where this work was completed, for kind hospitality and partial support. The work of V.M.M. was partially supported by the Russian Government Program of Competitive Growth of Kazan Federal University.

- 
- [1] M. I. Katsnelson, *Graphene: Carbon in Two Dimensions* (Cambridge University Press, Cambridge, 2012).
  - [2] *Physics of Graphene*, ed. H. Aoki and M. S. Dresselhaus (Springer, Cham, 2014).
  - [3] V. A. Parsegian, *Van der Waals Forces: A Handbook for Biologists, Chemists, Engineers, and Physicists* (Cambridge University Press, Cambridge, 2005).
  - [4] M. Bordag, G. L. Klimchitskaya, U. Mohideen, and V. M. Mostepanenko, *Advances in the Casimir Effect* (Oxford University Press, Oxford, 2015).

- [5] A. H. Castro Neto, F. Guinea, N. M. R. Peres, K. S. Novoselov, and A. K. Geim, *Rev. Mod. Phys.* **81**, 109 (2009).
- [6] J. F. Dobson, A. White, and A. Rubio, *Phys. Rev. Lett.* **96**, 073201 (2006).
- [7] G. Gómez-Santos, *Phys. Rev. B* **80**, 245424 (2009).
- [8] D. Drosdoff and L. M. Woods, *Phys. Rev. B* **82**, 155459 (2010).
- [9] D. Drosdoff and L. M. Woods, *Phys. Rev. A* **84**, 062501 (2011).
- [10] Bo E. Sernelius, *Europhys. Lett.* **95**, 57003 (2011).
- [11] J. Sarabadani, A. Naji, R. Asgari, and R. Podgornik, *Phys. Rev. B* **84**, 155407 (2011); *Phys. Rev. B* **87**, 239905(E) (2013).
- [12] D. Drosdoff, A. D. Phan, L. M. Woods, I. V. Bondarev, and J. F. Dobson, *Eur. Phys. J. B* **85**, 365 (2012).
- [13] Bo E. Sernelius, *Phys. Rev. B* **85**, 195427 (2012).
- [14] A. D. Phan, L. M. Woods, D. Drosdoff, I. V. Bondarev, and N. A. Viet, *Appl. Phys. Lett.* **101**, 113118 (2012).
- [15] A. D. Phan, N. A. Viet, N. A. Poklonski, L. M. Woods, and C. H. Le, *Phys. Rev. B* **86**, 155419 (2012).
- [16] W.-K. Tse and A. H. Macdonald, *Phys. Rev. Lett.* **109**, 236806 (2012).
- [17] V. B. Svetovoy and G. Palasantzas, *Phys. Rev. Applied* **2**, 034006 (2014).
- [18] L. M. Woods, D. A. R. Dalvit, A. Tkatchenko, P. Rodrigues-Lopez, A. W. Rodrigues, and R. Podgornik, *Rev. Mod. Phys.* **88**, 045003 (2016).
- [19] C. Abbas, B. Guizal, and M. Antezza, *Phys. Rev. Lett.* **118**, 126101 (2017).
- [20] T. E. Judd, R. G. Scott, A. M. Martin, B. Kaczmarek, and T. M. Fromhold, *New J. Phys.* **13**, 083020 (2011).
- [21] T. Cysne, W. J. M. Kort-Kamp, D. Oliver, F. A. Pinheiro, F. S. S. Rosa, and C. Farina, *Phys. Rev. A* **90**, 052511 (2014).
- [22] N. Knusnutdinov, R. Kashapov, and L. M. Woods, *Phys. Rev. A* **94**, 012513 (2016).
- [23] T. P. Cysne, T. G. Rappoport, A. Ferreira, J. M. Viana Parente Lopes, and N. R. M. Peres, *Phys. Rev. B* **94**, 235405 (2016).
- [24] N. S. Nichols, A. Del Maestro, C. Wexler, and V. N. Kotov, *Phys. Rev. B* **93**, 205412 (2016).
- [25] E. Eizner, B. Horovitz, and C. Henkel, *Eur. Phys. J. D* **66**, 321 (2012).
- [26] E. M. Lifshitz and L. P. Pitaevskii, *Statistical Physics, Part II* (Pergamon, Oxford, 1980).

- [27] M. Bordag, I. V. Fialkovsky, D. M. Gitman, and D. V. Vassilevich, Phys. Rev. B **80**, 245406 (2009).
- [28] I. V. Fialkovsky, V. N. Marachevsky, and D. V. Vassilevich, Phys. Rev. B **84**, 035446 (2011).
- [29] M. Bordag, G. L. Klimchitskaya, and V. M. Mostepanenko, Phys. Rev. B **86**, 165429 (2012).
- [30] G. L. Klimchitskaya and V. M. Mostepanenko, Phys. Rev. B **87**, 075439 (2013).
- [31] G. L. Klimchitskaya and V. M. Mostepanenko, Phys. Rev. B **89**, 035407 (2014).
- [32] G. L. Klimchitskaya, V. M. Mostepanenko, and Bo E. Sernelius, Phys. Rev. B **89**, 125407 (2014).
- [33] G. L. Klimchitskaya, U. Mohideen, and V. M. Mostepanenko, Phys. Rev. B **89**, 115419 (2014).
- [34] G. L. Klimchitskaya and V. M. Mostepanenko, Phys. Rev. A **89**, 052512 (2014).
- [35] A. A. Banishev, H. Wen, J. Xu, R. K. Kawakami, G. L. Klimchitskaya, V. M. Mostepanenko, and U. Mohideen, Phys. Rev. B **87**, 205433 (2013).
- [36] M. Chaichian, G. L. Klimchitskaya, V. M. Mostepanenko, and A. Tureanu, Phys. Rev. A **86**, 012515 (2012).
- [37] B. Arora, H. Kaur, and B. K. Sahoo, J. Phys. B **47**, 155002 (2014).
- [38] K. Kaur, J. Kaur, B. Arora, and B. K. Sahoo, Phys. Rev. B **90**, 245405 (2014).
- [39] K. Kaur, B. Arora, and B. K. Sahoo, Phys. Rev. A **92**, 032704 (2015).
- [40] G. L. Klimchitskaya and V. M. Mostepanenko, Phys. Rev. A **89**, 062508 (2014).
- [41] G. L. Klimchitskaya and V. M. Mostepanenko, Phys. Rev. A **89**, 012516 (2014).
- [42] M. Bordag, G. L. Klimchitskaya, V. M. Mostepanenko, and V. M. Petrov, Phys. Rev. D **91**, 045037 (2015); **93**, 089907(E) (2016).
- [43] G. L. Klimchitskaya and V. M. Mostepanenko, Phys. Rev. B **91**, 174501 (2015).
- [44] V. B. Bezerra, G. L. Klimchitskaya, V. M. Mostepanenko, and C. Romero, Phys. Rev. A **94**, 042501 (2016).
- [45] G. L. Klimchitskaya, Int. J. Mod. Phys. A **31**, 1641026 (2016).
- [46] G. Bimonte, G. L. Klimchitskaya, and V. M. Mostepanenko, Phys. Rev. A **96**, 012517 (2017).
- [47] G. L. Klimchitskaya and V. M. Mostepanenko, Phys. Rev. B **93**, 245419 (2016).
- [48] G. L. Klimchitskaya and V. M. Mostepanenko, Phys. Rev. B **94**, 195405 (2016).
- [49] G. L. Klimchitskaya, C. C. Korikov, and V. M. Petrov, Phys. Rev. B **92**, 125419 (2015); **93**, 159906(E) (2016).
- [50] G. L. Klimchitskaya and V. M. Mostepanenko, Phys. Rev. A **93**, 052106 (2016).

- [51] G. L. Klimchitskaya and V. M. Mostepanenko, Phys. Rev. B **95**, 035425 (2017).
- [52] M. Bordag, I. Fialkovskiy, and D. Vassilevich, Phys. Rev. B **93**, 075414 (2016); **95**, 119905(E) (2017).
- [53] G. Bimonte, G. L. Klimchitskaya, and V. M. Mostepanenko, Phys. Rev. B **96**, 115430 (2017).
- [54] T. Stauber, N. M. R. Peres, and A. K. Geim, Phys. Rev. B **78**, 085432 (2008).
- [55] V. Druzhinina and M. DeKieviet, Phys. Rev. Lett. **91**, 193202 (2004).
- [56] H. Oberst, Y. Tashiro, K. Shimizu, and F. Shimizu, Phys. Rev. A **71**, 052901 (2005).
- [57] V. N. Marachevsky, J. Phys. A: Math. Theor. **45**, 374021 (2012).
- [58] Z.-C. Yan and J. F. Babb, Phys. Rev. A **58**, 1247 (1998).
- [59] J. F. Babb, G. L. Klimchitskaya, and V. M. Mostepanenko, Phys. Rev. A **70**, 042901 (2004).
- [60] R. Brühl, P. Fouquet, R. E. Grisenti, J. P. Toennies, G. C. Hegerfeldt, T. Köhler, M. Stoll, and C. Walter, Europhys. Lett. **59**, 357 (2002).
- [61] G. Vidali and M. W. Cole, Surf. Sci. **110**, 10 (1981).
- [62] A. O. Caride, G. L. Klimchitskaya, V. M. Mostepanenko, and S. I. Zanette, Phys. Rev. A **71**, 042901 (2005).
- [63] L. A. Falkovsky, J. Phys.: Conf. Series **129**, 012004 (2008).
- [64] P. K. Pyatkovskiy, J. Phys.: Condens. Matter **21**, 025506 (2009).
- [65] V. P. Gusynin, S. G. Sharapov, and J. P. Carbotte, New J. Phys. **11**, 095013 (2009).
- [66] S. A. Jafari, J. Phys.: Condens. Matter **24**, 205802 (2012).
- [67] K. F. Mak, M. Y. Sfeir, Y. Wu, C. H. Lui, J. A. Misewich, and T. F. Heinz, Phys. Rev. Lett. **101**, 196405 (2008).
- [68] D. B. Hough and L. R. White, Adv. Coll. Interface Sci. **14**, 3 (1980).
- [69] L. Bergström, Adv. Coll. Interface Sci. **70**, 125 (1997).
- [70] G. M. Obrecht, R. J. Wild, M. Antezza, L. P. Pitaevskii, S. Stringari, and E. A. Cornell, Phys. Rev. Lett. **98**, 063201 (2007).
- [71] H. Haakh, F. Intravaia, C. Henkel, S. Spagnolo, R. Passante, B. Pover, and F. Sols, Phys. Rev. A **80**, 062905 (2009).
- [72] J. Schiefele and C. Henkel, Phys. Rev. A **82**, 023605 (2010).
- [73] V. B. Bezerra, G. L. Klimchitskaya, V. M. Mostepanenko, and C. Romero, Phys. Rev. D **81**, 055003 (2010).
- [74] V. B. Bezerra, G. L. Klimchitskaya, V. M. Mostepanenko, and C. Romero, Phys. Rev. D **89**,

035010 (2014).

- [75] H. R. Haakh, C. Henkel, S. Spagnolo, L. Rizzuto, and R. Passante, *Phys. Rev. A* **89**, 022509 (2014).
- [76] D. E. Chang, K. Sinha, J. M. Taylor, and H. J. Kimble, *Nature Commun.* **5**, 4343 (2014).
- [77] H. Bender, C. Stehle, C. Zimmermann, S. Slama, J. Fiedler, S. Scheel, S. Y. Buhmann, and V. N. Marachevsky, *Phys. Rev. X* **4**, 011029 (2014).
- [78] M. Köhne, R. Bennett, T. Reisinger, and S. Y. Buhmann, *Phys. Rev. A* **96**, 013626 (2017).

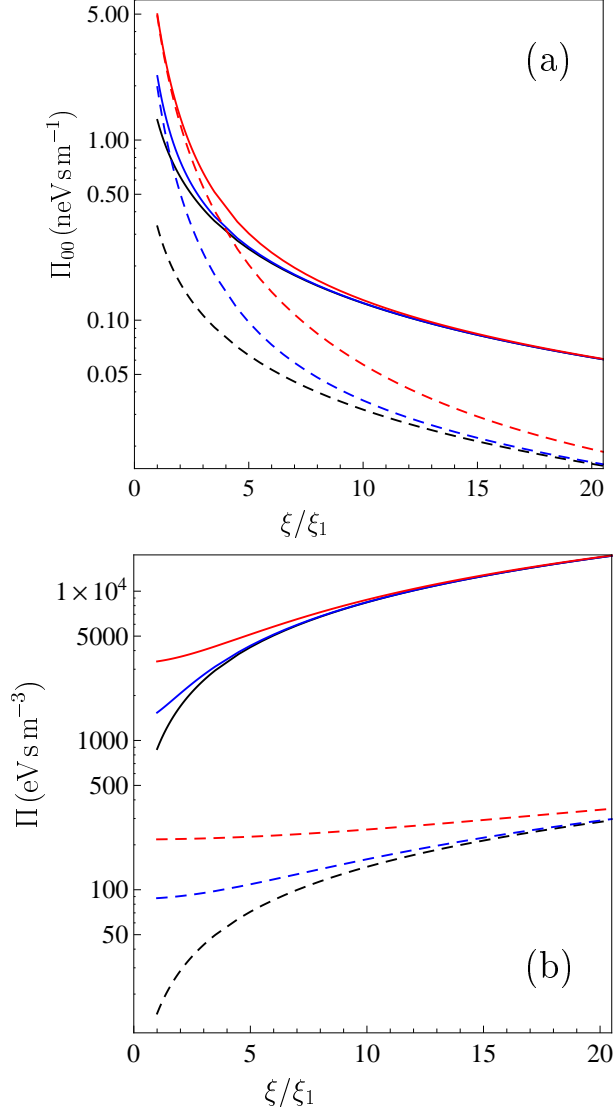


FIG. 1: (a) The 00-component of the polarization tensor  $\Pi_{00}$  and (b) the combination of its components  $\Pi$  are shown at  $T = 300\text{ K}$  (the solid lines) and at  $T = 77\text{ K}$  (the dashed lines) for  $k_{\perp} = 10\xi_1/c$  as functions of  $\xi/\xi_1$  along the imaginary frequency axis for  $\xi \geq \xi_1$ . The lines of each kind from bottom to top are plotted for a gapless graphene with  $\mu = 0, 0.2, \text{ and } 0.5\text{ eV}$ , respectively. Here and in all other figures, we take for the Fermi velocity the value  $v_F = c/300$ .

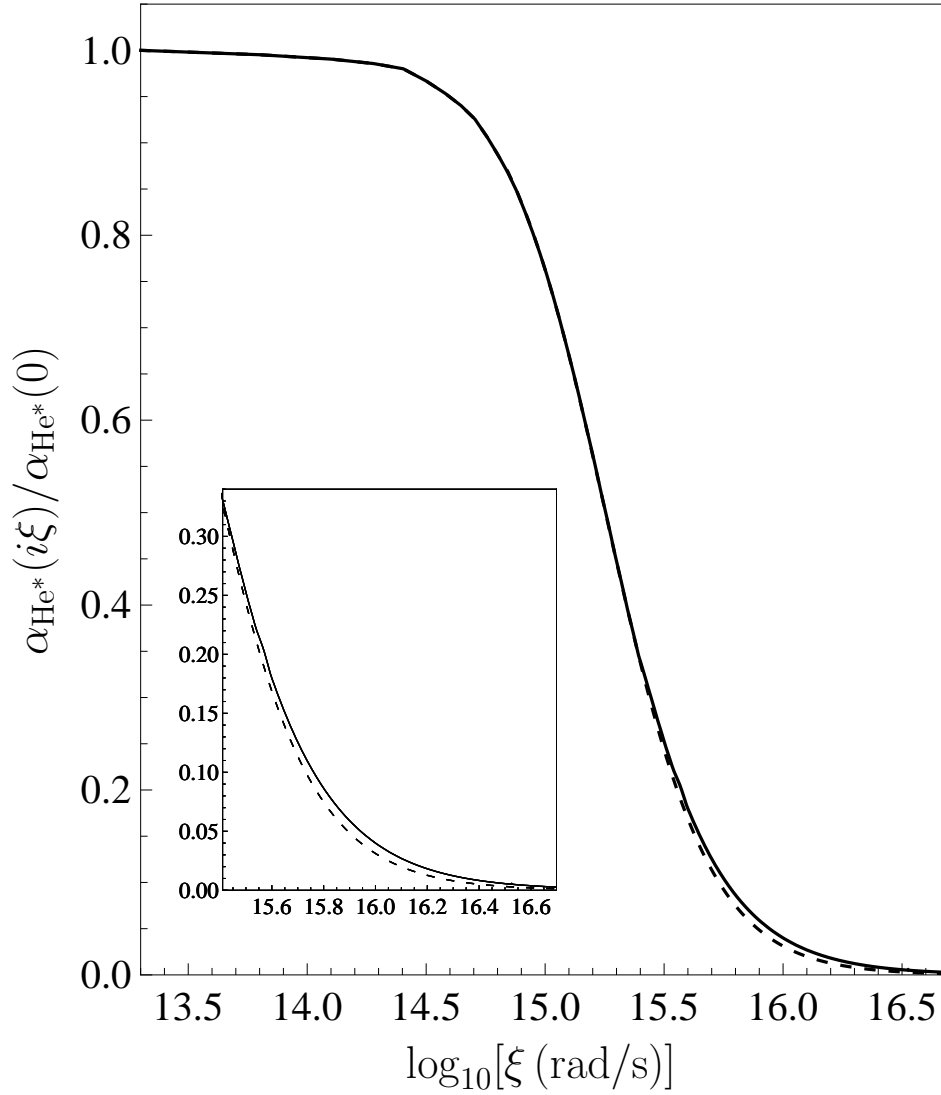


FIG. 2: The highly-accurate and single-oscillator dynamic atomic polarizabilities of He\* normalized to their static value are shown as functions of the imaginary frequency by the solid and dashed lines, respectively. The region of high frequencies is presented on an enlarged scale in the inset.



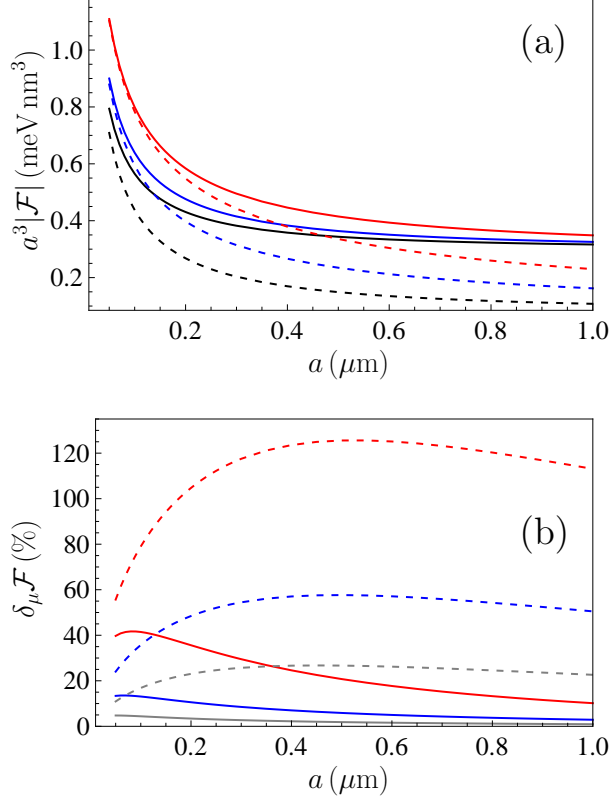


FIG. 3: (a) The magnitudes of the Casimir-Polder free energy multiplied by the third power of separation between an atom of  $\text{He}^*$  and a gapless graphene are shown as functions of separation at  $T = 300\text{ K}$  (the solid lines) and  $T = 77\text{ K}$  (the dashed lines). The lines of each kind from bottom to top are plotted for graphene with  $\mu = 0, 0.2, \text{ and } 0.5\text{ eV}$ , respectively. (b) The relative changes in the Casimir-Polder free energy due to nonzero chemical potential are shown as functions of separation by the solid and dashed lines at  $T = 300\text{ K}$  and  $T = 77\text{ K}$ , respectively. The lines of each kind from bottom to top are for graphene with  $\mu = 0.1, 0.2, \text{ and } 0.5\text{ eV}$ , respectively.

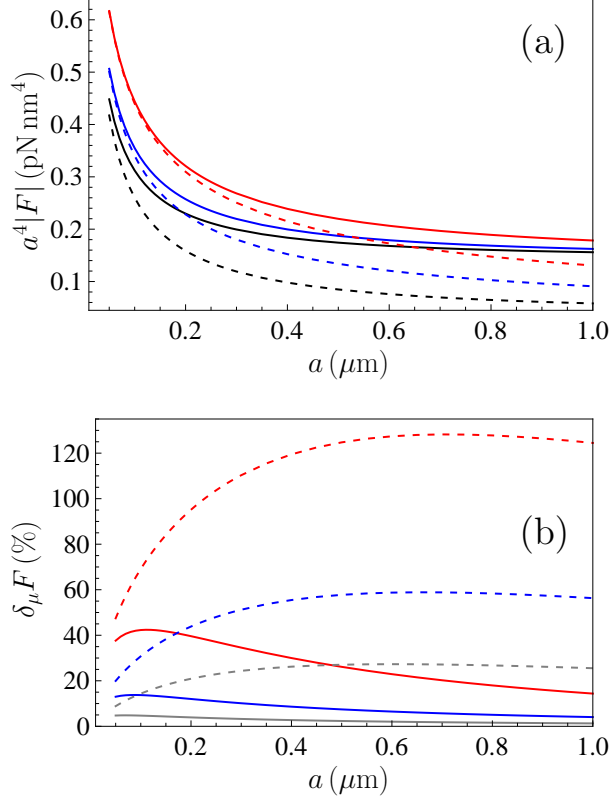


FIG. 4: (a) The magnitudes of the Casimir-Polder force multiplied by the fourth power of separation between an atom of He\* and a gapless graphene are shown as functions of separation at  $T = 300$  K (the solid lines) and  $T = 77$  K (the dashed lines). The lines of each kind from bottom to top are plotted for graphene with  $\mu = 0, 0.2, \text{ and } 0.5$  eV, respectively. (b) The relative changes in the Casimir-Polder force due to nonzero chemical potential are shown as functions of separation by the solid and dashed lines at  $T = 300$  K and  $T = 77$  K, respectively. The lines of each kind from bottom to top are for graphene with  $\mu = 0.1, 0.2, \text{ and } 0.5$  eV, respectively.

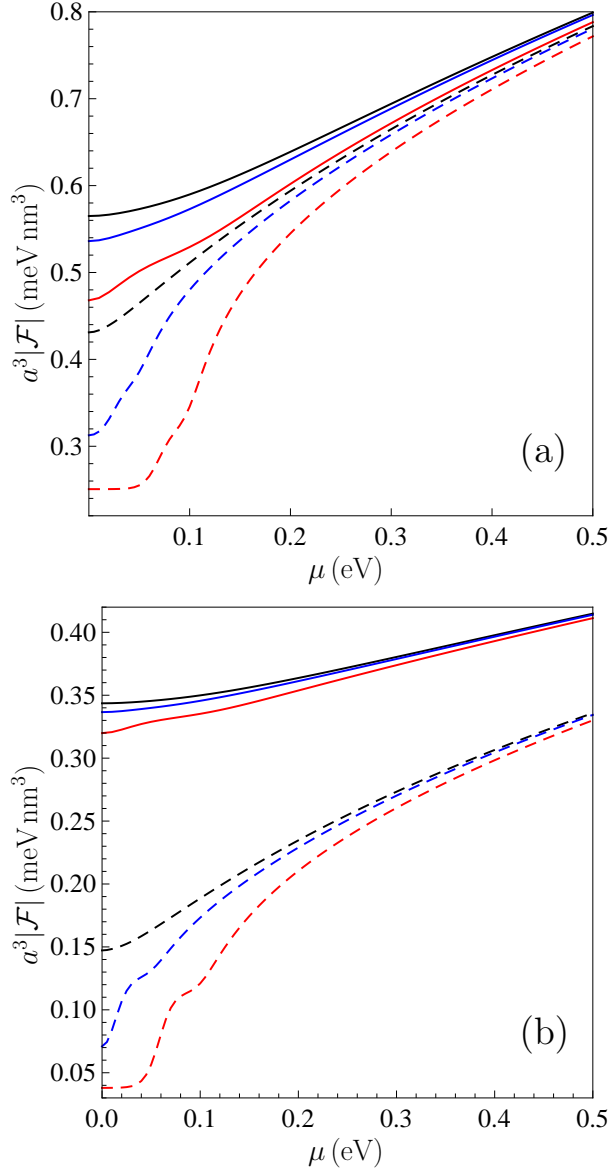


FIG. 5: (a) The magnitudes of the Casimir-Polder free energy multiplied by the third power of separation between an atom of  $\text{He}^*$  and gapped graphene are shown at  $T = 300\text{ K}$  (the solid lines) and  $T = 77\text{ K}$  (the dashed lines) as functions of chemical potential for (a)  $a = 100\text{ nm}$  and (b)  $a = 500\text{ nm}$ . The lines of each kind from bottom to top are plotted for graphene with  $\Delta = 0.2, 0.1,$  and  $0\text{ eV}$ , respectively.

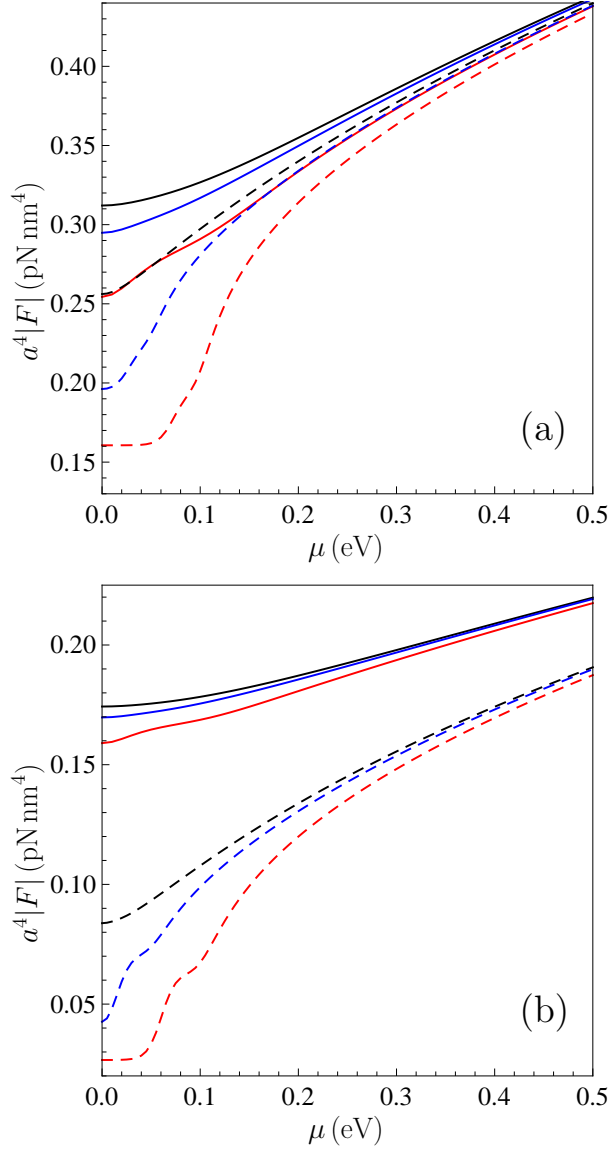


FIG. 6: (a) The magnitudes of the Casimir-Polder force multiplied by the fourth power of separation between an atom of  $\text{He}^*$  and gapped graphene are shown at  $T = 300$  K (the solid lines) and  $T = 77$  K (the dashed lines) as functions of chemical potential for (a)  $a = 100$  nm and (b)  $a = 500$  nm. The lines of each kind from bottom to top are plotted for graphene with  $\Delta = 0.2, 0.1,$  and  $0$  eV, respectively.

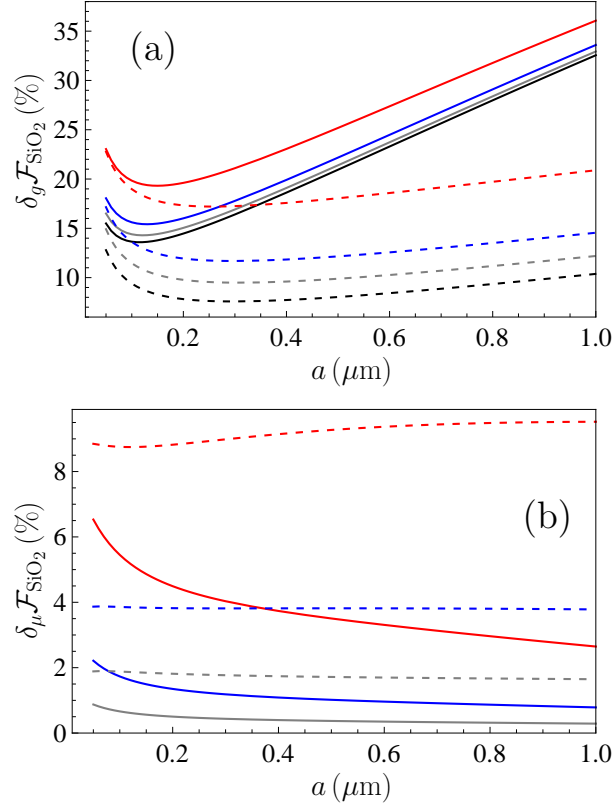


FIG. 7: The relative changes in the Casimir-Polder free energy for an atom of  $\text{He}^*$  interacting with a gapless graphene deposited on a  $\text{SiO}_2$  substrate due to (a) the presence of graphene (the solid and dashed lines considered from bottom to top are for  $\mu=0, 0.1, 0.2,$  and  $0.5$  eV, respectively) and (b) the nonzero chemical potential (the solid and dashed lines considered from bottom to top are for  $\mu=0.1, 0.2,$  and  $0.5$  eV, respectively) are shown as functions of separation. The solid lines are computed at  $T = 300$  K and the dashed ones at  $T = 77$  K.

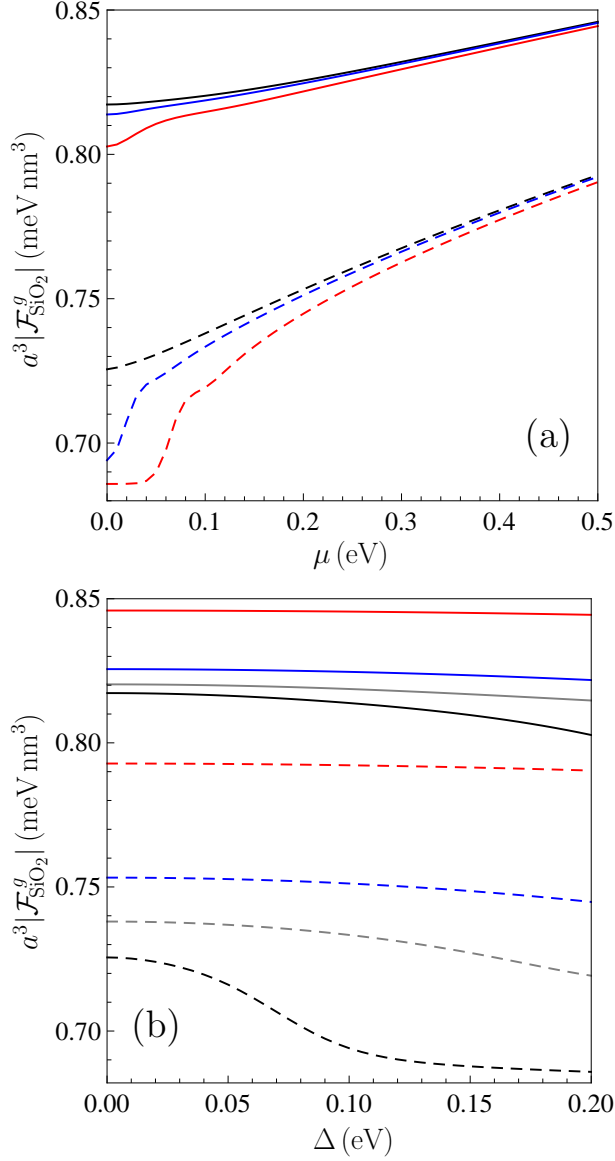


FIG. 8: The magnitudes of the Casimir-Polder free energy multiplied by the third power of separation  $a=0.5\mu\text{m}$  between an atom of  $\text{He}^*$  and graphene-coated  $\text{SiO}_2$  substrate are shown at  $T = 300\text{ K}$  (the solid lines) and at  $T = 77\text{ K}$  (the dashed lines) as functions of (a) the chemical potential and (b) the mass-gap parameter. The lines of each kind from bottom to top are plotted for graphene with (a)  $\Delta = 0.2, 0.1,$  and  $0\text{ eV}$  and (b)  $\mu = 0.01, 0.2,$  and  $0.5\text{ eV}$ , respectively.

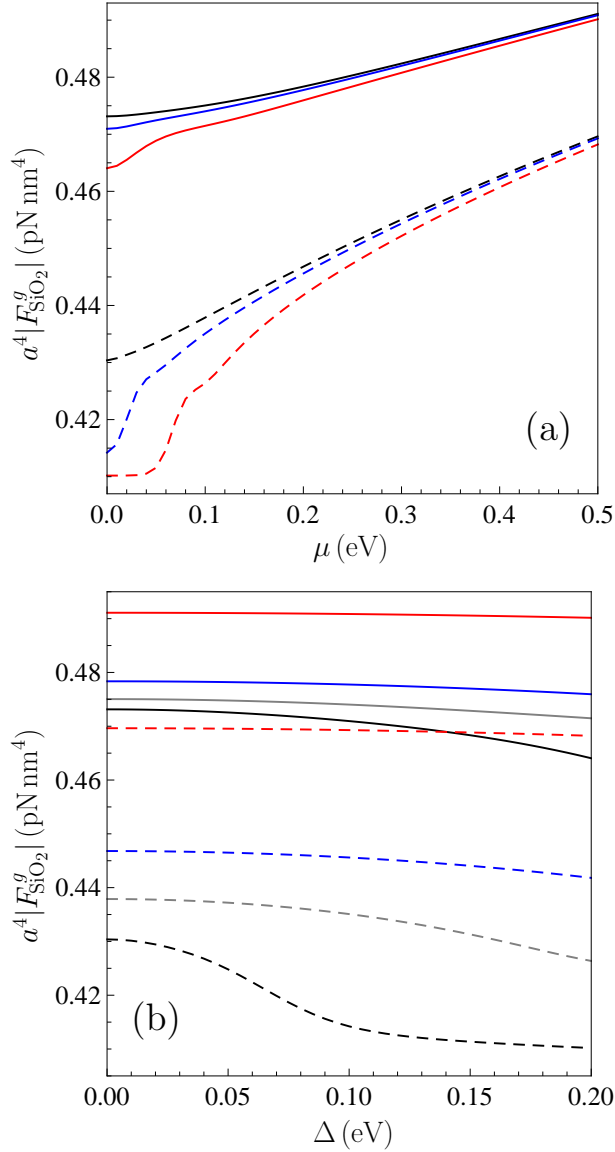


FIG. 9: The magnitudes of the Casimir-Polder force multiplied by the fourth power of separation  $a=0.5\mu\text{m}$  between an atom of  $\text{He}^*$  and graphene-coated  $\text{SiO}_2$  substrate are shown at  $T = 300\text{ K}$  (the solid lines) and at  $T = 77\text{ K}$  (the dashed lines) as functions of (a) the chemical potential and (b) the mass-gap parameter. The lines of each kind from bottom to top are plotted for graphene with (a)  $\Delta = 0.2, 0.1,$  and  $0\text{ eV}$  and (b)  $\mu = 0.01, 0.2,$  and  $0.5\text{ eV}$ , respectively.